A NEW DIRECTION-FINDING SYSTEM FOR AURORAL HISS IN ANTARCTICA BASED ON THE MEASUREMENT OF TIME DIFFERENCE OF WAVE ARRIVAL AT THREE SPACED OBSERVING POINTS

Masanori NISHINO, Yoshihito TANAKA, Akira IWAI,
Toshiaki YAMAGUCHI, Tetsuo KAMADA

Research Institute of Atmospherics, Nagoya University, 13, Honohara 3-chome, Toyokawa 442

and

Takeo HIRASAWA

National Institute of Polar Research, 9–10, Kaga 1-chome, Itabashi-ku, Tokyo 173

Abstract: A newly developed direction finding ("DF") for auroral hiss based on the measurement of time difference of wave arrival was carried out in 1978 at Syowa Station (geomag. lat. −70.4°), Antarctica and its two slave unmanned observing points located at about 20 km from Syowa Station. The auroral hiss signals received at the two spaced points were transmitted to Syowa Station by 2 GHz telemeters. The arrival time difference of auroral hiss between Syowa Station and each spaced point was automatically determined by cross-correlating the waveforms of the received signals.

It has been found that the new DF can determine localized exit regions at the ionospheric level which show a rapid temporal movement. A comparison of the DF results with ground-based auroral data has shown that impulsive type auroral hiss with a wide frequency range larger than several tens kHz has not emerged from the whole region of bright aurora but from some localized regions of bright auroras at the ionospheric level, and that the arrival directions of auroral hiss change rapidly in accordance with the auroral movements.

The time resolution of the new DF is about 3 μs by the measurement of delay times between two observing points in the reception of NAA wave. Therefore, the incident and azimuthal angles were measured with an accuracy of about 10° in the range of incident angle of 20° to 80°.

1. Introduction

Direction finding ("DF") of VLF emissions is essential to study their generation mechanism and propagation path. DF has been made in different ways; a goniometer DF by crossed loop antennas, a DF based on the analysis of magnetic and electric

fields received by crossed loops and vertical antenna, and a DF based on measurements of time differences of wave arrival.

ELLIS and CARTWRIGHT (1959) first observed the arrival direction of mid-latitude VLF emissions using the goniometer method. This goniometer DF is generally applicable to linearly polarized waves, but it is useless for auroral hiss which propagates downwards with elliptical wave polarization.

TANAKA (1972) has observed the arrival direction of auroral VLF hiss at Syowa Station, using a DF method based on the analysis of Lissajous' figures of electric and magnetic fields displayed on cathode ray tubes. This DF method requires a narrow-band reception because of the validity of the DF for monochromatic waves. The measuring accuracy of the arrival direction was often decreased by ringing effects of the narrow-band receivers ($Q=200$) caused by impulsive atmospherics, the peak intensity of which was usually about two orders in magnitude over that of auroral VLF hiss. Adopting an algebraic computation method, TSURUDA and HAYASHI (1975) have developed a DF system to be applicable to elliptically polarized waves. MAKITA (1979) has applied this DF system to auroral hiss DF at Syowa Station. The measuring accuracy of this DF system depends strongly on wave polarization as well as on incident angle.

DELLOUE *et al.* (1963) used the DF based on the measurement of time differences of wave arrival at spaced observing points to determine the exits of whistlers at the lower ionospheric level. There are difficulties that whistlers and VLF emissions have usually no distinct onset mark to ensure the measuring accuracy of the DF.

We have developed a DF for auroral VLF hiss based on the measurement of time difference of wave arrival, which is independent of wave polarization as well as of waveform. The arrival time differences among the signals received at three spaced observing points are determined by computing the cross-correlation among the received wide-band signals, so that the interference of impulsive atmospherics is reduced. We describe our new DF system and demonstrate the effectiveness of this DF system. Some preliminary results of arrival direction of auroral hiss are presented and are discussed with reference to the ground-based auroral data.

2. Direction-Finding System

Fig. 1 shows the configuration of the three observing points and the block diagram of the DF system. The three observing points are composed of the main point (M) at Syowa Station (geographic lat. $-69.03°$, long. $39.60°$ and geomagnetic lat. $-70.38°$, long. $79.39°$) on East Ongul Island, a remote unmanned point (S_1) at 30 m above the sea level at Langhovde, and a second one (S_2) on the ice slope of the Antarctic Continent at 430 m above the sea level. The distance between M and S_1 is 19.2 km and that between M and S_2 is 18.2 km. The intersecting angle between the two base lines (M-S_1 and M-S_2) is $80.0°$.

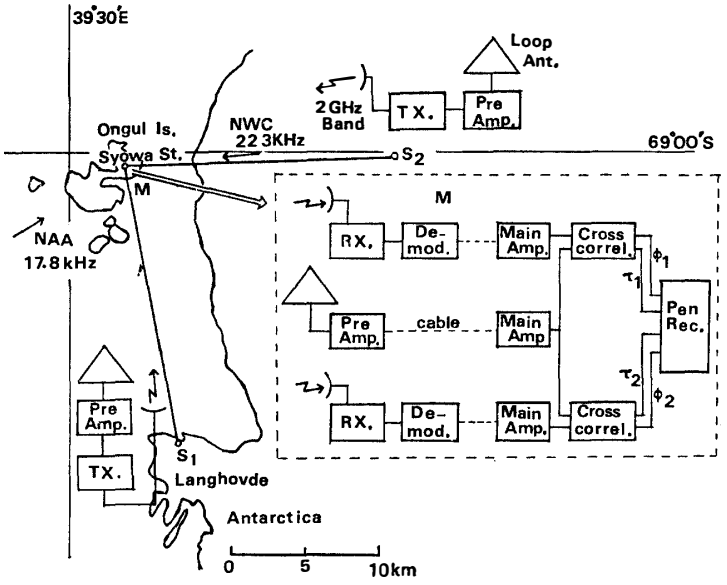

Fig. 1. DF system for auroral hiss based on the measurement of time differences of wave arrival; configuration of the three spaced observing points (M, S_1 and S_2) and the block diagram of the DF system.

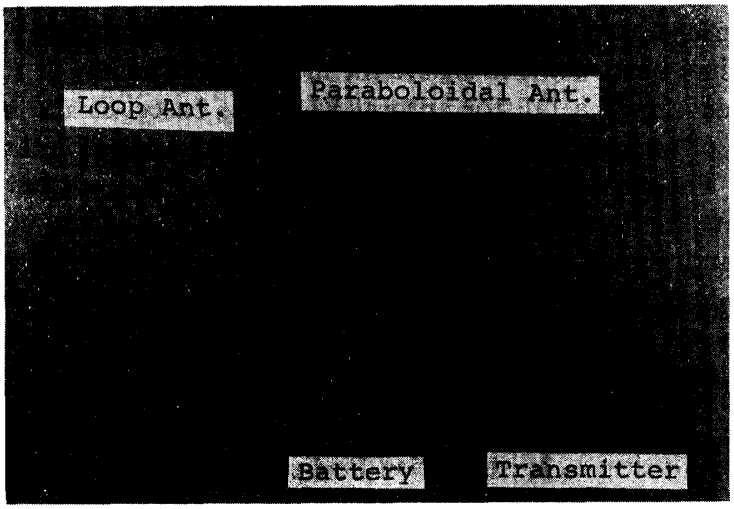

Fig. 2. Loop antenna and paraboloidal transmitting antenna at the unmanned observing point (S_2).

Auroral hiss signals over the intensity of flux density 10^{-16} W/m²Hz received at the unmanned point by the two-turn delta loop antenna, 8 m high and 14 m at the base, are transmitted by 2 GHz telemeter to Syowa Station. Fig. 2 shows the loop antenna, the paraboloidal transmitting antenna, 2 GHz transmitter and the battery box installed at the unmanned observing point S_2.

Table 1. Performance of the transmitter-receiver (NEC TR-2G960).

(1)	Transmitter-receiver	
	Transmission frequency	S_1-M, 1989 MHz
		S_2-M, 1859 MHz
	Modulation	FM
	Transmission frequency band	0.3–100 kHz
	Frequency deviation	200 kHzrms
(2)	Transmitter	
	Power	0.3 W
	Frequency stability	$<\pm 8\times 10^{-5}$
(3)	Receiver	
	Noise figure	7.5 dB
	Intermediate frequency	70 MHz
	Frequency stability	$<\pm 5\times 10^{-5}$
(4)	Power consumption	
	Transmitter	<4 W
	Receiver	<7 W

Table 2. Performance of transmission lines from the slave points (S_1 and S_2) to the receiving point at Syowa Station.

(1)	TX output power	24.8 dBm	0.3 W
(2)	Propagation loss	−127.5 dB	M-S_1 (18.9 km)
		−124.5 dB	M-S_2 (18.5 km)
(3)	Feeder loss	−2.0 dB	TX, 8D2W, 5 m
		−2.0 dB	RX, 8D2W, 5 m
(4)	Antenna gain	24.2 dB	TX, 1.2 mϕ, paraboloidal antenna
		24.2 dB	RX, 1.2 mϕ, paraboloidal antenna
(5)	Line loss	−83.1 dB	M-S_1, (2)+(3) (TX+RX)+(4) (TX+RX)
		−80.1 dB	M-S_2, (2)+(3) (TX+RX)+(4) (TX+RX)
(6)	RX receiving power	−58.3 dBm	M-S_1, (1)+(5)
		−55.3 dBm	M-S_2, (1)+(5)
(7)	Receiver noise	−94.7 dBm	B=15 MHz, NF=7.5 dB
(8)	Carrier to noise ratio (C/N)	36.4 dB	M-S_1, (6)−(7)
		39.4 dB	M-S_2, (6)−(7)
(9)	Improvement factor of signal to noise ratio (S/N)	32.6 dB	FM improvement factor
(10)	S/N of the lines	69.0 dB	M-S_1, (8)+(9)
		72.0 dB	M-S_2, (8)+(9)

The performance characteristics of the transmitter-receiver are shown in Table 1, and those for the transmission lines in Table 2. The electric power of the unmanned points was supplied by the battery composed of air-polarized layerbuilt type dry cell (YUASA LSA-1035) from the viewpoints of low power consumption and low atmospheric temperature ($-30°C$) at Antarctica.

3. Determination of Time Differences of Wave Arrival

As the spectral intensity of auroral hiss shows a maximum at a frequency between 5 and 20 kHz, the distance from Syowa Station (M) to each of the unmanned observing points (S_1 and S_2) has been chosen to be about 20 km corresponding to an average wavelength in this frequency range. Fig. 3 represents a schematic diagram to show

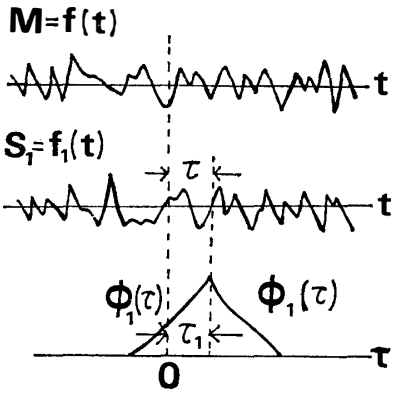

Fig. 3. Principle of the measurement of time differences of wave arrival between the two observing points (M and S_1), by cross-correlating the both waveforms.

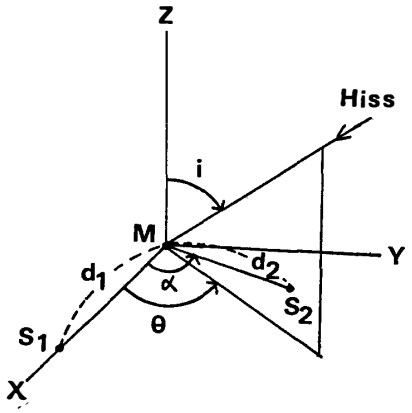

Fig. 4. Coordinate system of the measurement of azimuthal and incident angles.

the method for determining the arrival time difference between hiss signals received at the two points (M and S_1). When the waveform received at M is cross-correlated with that at S_1 shifted from 0 to τ along the time axis (t), the cross-correlation function $\phi_1(\tau)$ is defined by

$$\phi_1(\tau)=\lim_{T\to\infty}\int_0^T f(t)f_1(t+\tau)dt.$$

When the cross-correlation function $\phi_1(\tau)$ between the wave-form at S_1 and that at M becomes maximum by taking the time-lag (τ) as τ_1 ($\tau=\tau_1$), the time-lag (τ_1) can be considered as the time difference of wave arrival between M and S_1. By means of

(τ_1) and the other time difference (τ_2) of wave arrival between M and S_2, the azimuthal angle (θ) and the incident angle (i) shown in the coordinate system of Fig. 4, when auroral hiss arrives as a plane wave, are given by,

$$\tan\theta=\frac{\tau_2 d_1}{\tau_1 d_2}\operatorname{cosec}\alpha-\cot\alpha,$$

$$\sin i=c\operatorname{cosec}\alpha\sqrt{\left(\frac{\tau_1}{d_1}\right)^2+\left(\frac{\tau_2}{d_2}\right)^2-2\left(\frac{\tau_1\tau_2}{d_1 d_2}\right)\cos\alpha},$$

where c is the light velocity, d_1 is the distance between M and S_1, d_2 is the distance between M and S_2, and α is the intersecting angle between the two base lines (M-S_1 and M-S_2).

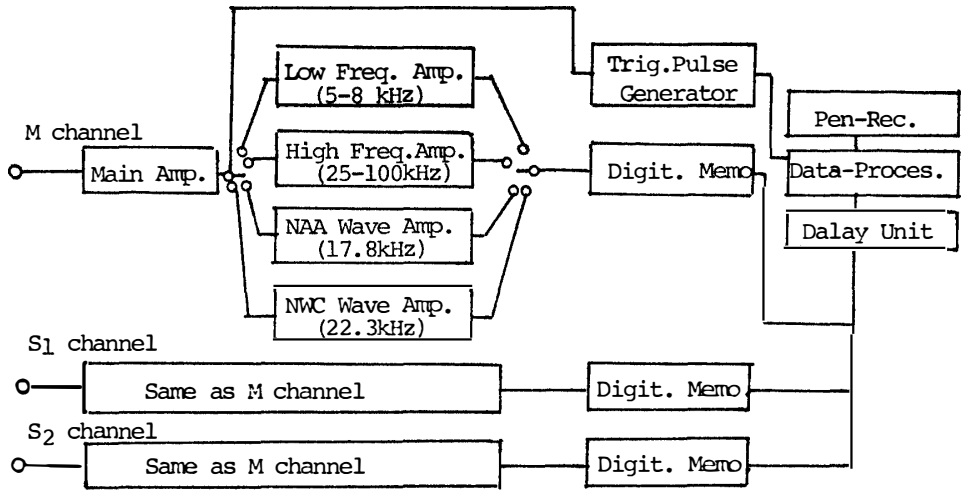

Fig. 5. Block diagram of DF analyzer; hiss receivers and correlator installed at Syowa Station.

Fig. 5 shows the block diagram of the DF analyzer installed at Syowa Station, which consists of the receivers for auroral hiss and VLF communication waves (NAA, 17.8 kHz and NWC, 22.3 kHz), and of the correlator. In order to avoid the interference of VLF communication waves (OMEGA: 10.2, 11.3 and 13.6 kHz, NAA and NWC), the wide-band hiss signals (0.3–100 kHz) received at the three spaced observing points (M, S_1 and S_2) are divided into two frequency ranges; a lower frequency range of 5–8 kHz and a higher one of 25–100 kHz. The DF observations of auroral hiss were usually made in the lower frequency range of 5–8 kHz. NAA and NWC signals are available for calibrating the DF system because their arrival directions are known.

The correlator consists of three digital memories (IWATSU DM305) and a data processor (IWATSU SM1330). The performance characteristics of the digital memory are represented in Table 3, and those of the data processor in Table 4. The band

Table 3. Main performance of the digital memory (IWATSU DM305).

Memory capacity	8 bits 1024 words
Maximum conversion time of A–D converter	1 μs/word
Memory circuit	MOS STATIC RAM
Input voltage range	±0.1 V～±50 V
Input frequency band	DC-250 kHz
Reading	Automatic repeat

Table 4. Main performance of the data processor (IWATSU SM1330).

Memory circuit		Dynamic RAM, 16 bits × 12 k words
Function		Cross-correlation
Data acquisition time		5 μs/word
Computation time,	256 words	about 0.45 s (measured)
	512 words	about 0.83 s (measured)
	1024 words	about 1.60 s (measured)
Output	2 channels	Delay times (τ_1 and τ_2)
	2 channels	Cross-correlation values (ϕ_1 and ϕ_2)
Accuracy		3%
Resolution		1/4096, 12 bits

limited signal is fed to each digital memory, where the analog signal is converted to digital and are transferred to the data processor by clock pulses. Then the time differences of wave arrival (τ_1 and τ_2) and the cross-correlation values ($\phi_1(\tau_1)$ and $\phi_2(\tau_2)$) are calculated. These values are averaged and converted to analog and then recorded on a pen-recorder. The correlator is equipped with a trigger pulse generator to reduce the interference of atmospherics. In case when the level of atmospherics received at M exceeds a somewhat higher trigger level than that of the maximum intensity of auroral hiss, a trigger pulse is generated to stop the computation of cross-correlation.

4. Observed Results

Fig. 6 shows an example from the results of auroral hiss observations on June 14, 1978 at Syowa Station; (a) the intensity of auroral hiss at 8 kHz recorded by means of a minimum level reading circuit (TANAKA, 1972), (b) the continuous records of the maximum cross-correlation values ($A\phi_1(\tau_1)$ and $A\phi_2(\tau_2)$) in the 5–8 kHz frequency band where A is a scale factor decided arbitrarily with reference to the dynamic range of the receiving system, and (c) the estimated incident and azimuthal angles of hiss. When any auroral hiss does not occur (2217–2220 and 2225–2228

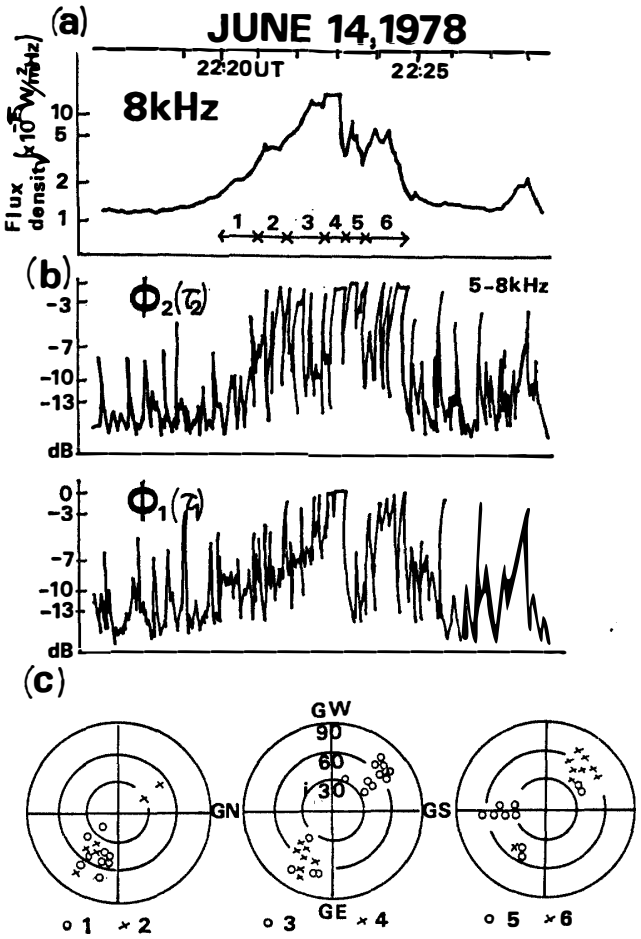

Fig. 6. Temporal evolution of observed results at 22 UT, June 14, 1978 at Syowa Station.
(a) Intensity of 8 kHz auroral hiss.
(b) Cross-correlation values of $A\phi_2(\tau_2)$ and $A\phi_1(\tau_1)$ for hiss signals at 5–8 kHz.
(c) Estimated azimuthal and incident angles of auroral hiss at 5–8 kHz. The numbers of 1–6 represent six sub-events.

UT), the maximum cross-correlation values show, from time to time, sharp spikes due to intense atmospherics, and fall immediately down to the zero level. When an auroral hiss begins to occur at 2220 UT, the minimum level envelopes of the cross-correlation values increase with the hiss activities, which seems to prove the effectiveness of the DF system. As illustrated on the panel (a), the hiss event with a duration of five minutes (2220–2225 UT) is divided into six sub-events with reference to the spike-type enhancements in hiss intensity variation. Based on the delay time data, the arrival directions of these sub-events are determined and shown on the panel (c). It is found from the results on the panels (a) and (c) that each spike-type sub-event appearing in the auroral hiss emission has emerged from a localized region at the ionospheric level, and that the localized region shifts with time.

The similar characteristics are also found in Fig. 7. On the panel (a) of Fig. 7, spike-type enhancements appear successively in the 5 kHz hiss intensity variation of 2010 to 2048 UT on May 24, 1978, which are characterized by ten sub-events. From the results of arrival directions on the panel (b), it is found that each sub-event is propagated from a localized region changing with time.

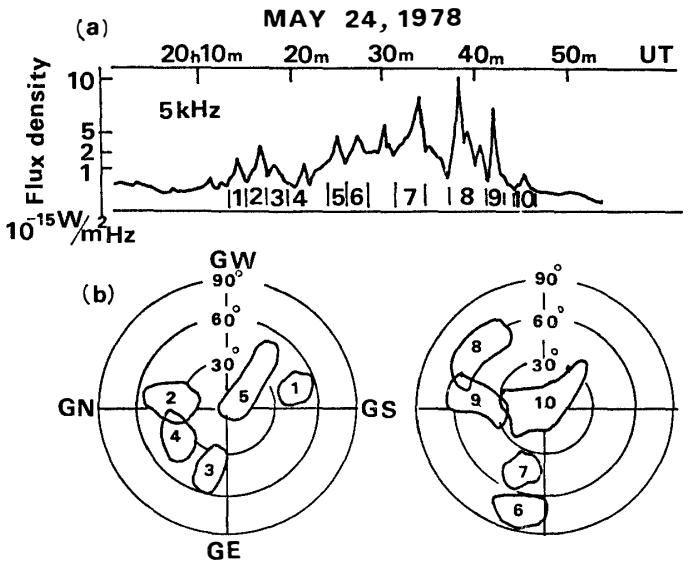

Fig. 7. Temporal evolution of observed results at 2010–2048 UT, May 24, 1978 at Syowa Station.

(a) Intensity of 8 kHz auroral hiss.

(b) Estimated azimuthal and incident angles of auroral at 5–8 kHz. The numbers of 1 to 10 represent ten sub-events.

From the above-mentioned results, it is found that our new DF system can detect a localized source of hiss which corresponds to each of sub-events composing an auroral hiss event, and changes with time. Hence, a comparison of arrival directions of hiss will be made significantly with auroral motions. The arrival directions of hiss are compared with the all-sky photographs of aurora for the following two events, where auroral hiss emissions occur in close association with large geomagnetic disturbances, and they are of impulsive type with a wide-band frequency range larger than several tens kHz, and during these events, active auroras appear with rapid changes in luminosity and in motion.

4.1. July 4, 1978 (Fig. 8)

An impulsive type auroral hiss started at 2246 UT simultaneously with a sharp negative decrease of the geomagnetic H component. The hiss event is divided into four sub-events shown on the panel (a) of Fig. 8. Each sub-event is propagated from a corresponding localized region, as shown on the panel (b). The arrival directions

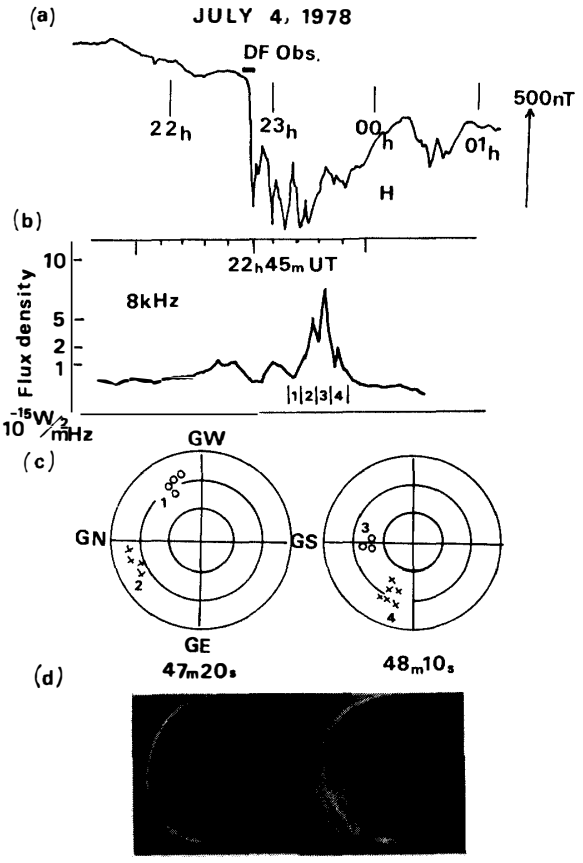

Fig. 8. Temporal evolution of observed results at 2246-2250 UT, July 4, 1978 at Syowa Station.
(a) Variation of geomagnetic H component at Syowa Station.
(b) Intensity of 8 kHz auroral hiss.
(c) Estimated azimuthal and incident angles of auroral hiss at 5–8 kHz.
(d) All-sky photographs of aurora.

of these four sub-events are compared with auroral behaviors illustrated in the two representative all-sky photographs of aurora on the panel (c), in the following.

(1) The auroral photograph (2247:20 UT) shows that folding form auroral arcs extend above the horizon from the geomagnetic west (GW) to the north (GN). Then, multi-band aurora appears near the horizon of the northeast (GNE). The auroral hiss emissions are first received at incident angles of about 70° from the GWNW direction, and then their azimuthal angles change from GWNW to GNNE.

(2) The aurora which brightens near the northern horizon suddenly expands towards the zenith at 2248:00 UT, as shown in the right-hand photograph. Associated with this auroral motion, the auroral hiss emissions arrive at incident angles of about 50° from the GN direction, and then their arrival directions change towards the GENE direction at incident angles of about 60°. These arrival directions of hiss are well accordant with the folding areas in active auroras. Subsequently, the intensity of hiss decreases with the wide expansion of bright aurora around the zenith, due to the heavy absorption of the hiss in the lower ionosphere ionized by precipitating auroral particles. The decay of the hiss intensity also corresponds to the maximum decrease of the geomagnetic *H* component.

4.2. June 26, 1978 (Fig. 9)

Relatively intense auroral hiss with a duration of about ten minutes occurs during the gradually decreasing phase of a large negative geomagnetic bay. During this hiss event, the auroral activity is variable in motion and in structure. In order to compare the arrival directions of hiss with the all-sky photographs of aurora, the hiss event is divided into nine sub-events with reference to spike-type enhancements in hiss intensity variation.

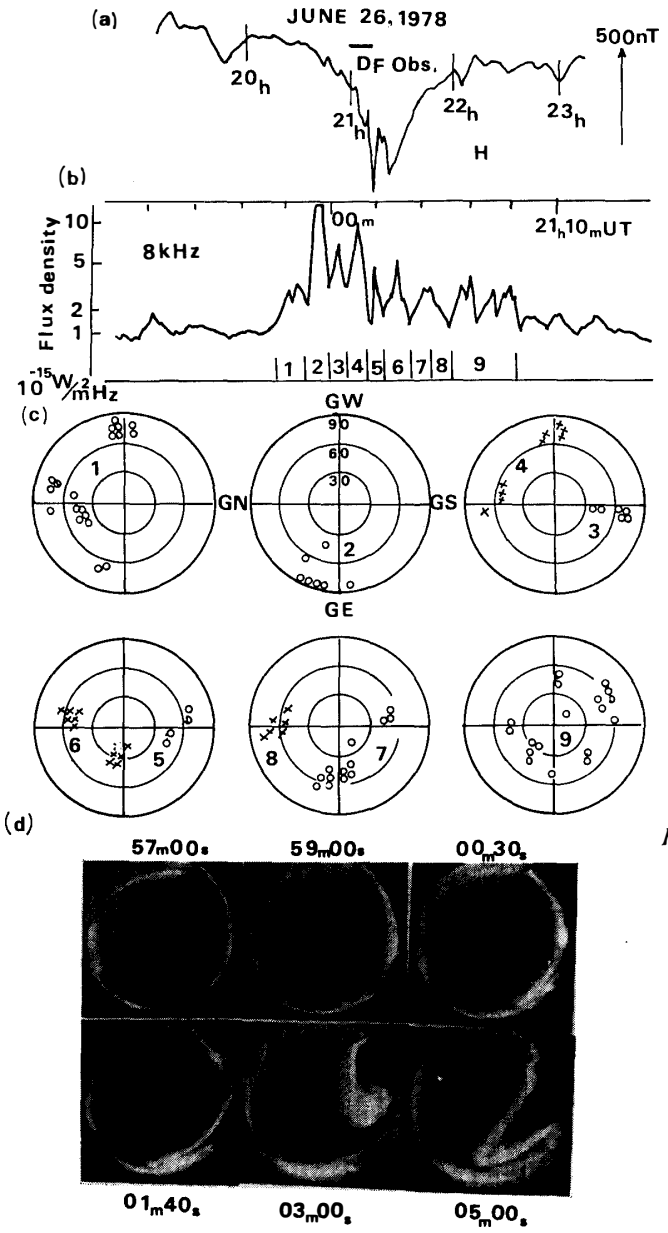

Fig. 9. Temporal evolution of observed results at 2057–2110 UT, June 26, 1978 at Syowa Station.
(a) Variation of geomagnetic H component at Syowa Station.
(b) Intensity of 8 kHz auroral hiss.
(c) Estimated azimuthal and incident angles of auroral hiss at 5–8 kHz.
(d) All-sky photographs of aurora.

(1) The all-sky photograph of aurora at 2057:00 UT shows multiple bands of aurora in the GW direction, dispersive rays in GN and a homogeneous band in GS of the horizontal center. Auroral hiss does not emerge from the occurrence region of the homogeneous band, but from the two regions of active multi-bands and rays mentioned above.

(2) Intense auroral hiss emissions (No. 2 sub-event) arrive from the region near the GE horizon, where a couple of movements of folding auroras are observed in the all-sky photograph at 2059:00 UT.

(3) As is clearly seen in the all-sky photographs at 2100:30, 2101:40, 2103:00 and 2105:00 UT, a bright auroral band becomes active above the GS horizon at 2100:30 UT, and then it begins to fold while moving rapidly eastwards. This auroral movement continues till 2105:00 UT, and the multi-band auroras expand towards the zenith. Corresponding to these auroral displays, the arrival directions of hiss (sub-events Nos. 3, 5, 7 and 9) change rapidly in accordance with the motion of the bright auroras.

(4) During the period from 2100:30 to 2105:00 UT, diffuse rays of aurora also become active in the region of the GN direction. Corresponding to these auroral activities, auroral hiss emissions are received from the GW and GN directions (Nos. 4, 6 and 8).

5. Summary and Discussion

It has been found from the observed results that our new DF based on the measurement of time differences of wave arrival at three spaced observing points can detect effectively a localized source of hiss which corresponds to each of sub-events composing an auroral hiss event, and changes with time. A comparison of the DF results of hiss with the ground-based auroral data has established that impulsive type auroral hisses have not emerged from quiet auroras but from some localized regions of bright auroras at the ionospheric level where we find rapid changes in luminosity and in motion.

OGUTI (1975) has analyzed real-time auroral records on a video tapes obtained by use of a highly sensitive TV camera at Syowa Station, and simultaneous records of VLF waves on the sound track of the same video tapes. He has identified the hiss emitting auroral activities by cross-correlation analysis between the temporal variations in luminosity of auroral structures and the temporal variations of hiss intensities; the auroral hiss is associated with specific characteristics of aurora, such as rapid brightening and rapid motions, and it is not associated with quiet auroras which have no remarkable motions and changes in luminosity.

The measuring accuracy of the DF depends on the time resolution in computing the cross-correlation. The maximum sampling speed of the digital memory (DM305) is 1 μs. It is difficult, however, to implement actually the time resolution of 1 μs

in finding the arrival direction of auroral hiss superimposed by interfering noises such as atmospherics and other background radio noises. The actual measuring accuracy was statistically deduced from the distribution of the delay times in the reception of NAA wave. The frequency distribution of this delay times was in shape of a normal distribution with its standard deviation of about 3 μs. Therefore, when the incident angle lies in the range of 20° to 80°, both incident and azimuthal angles can be determined with an accuracy of 10°. In the case of small incident angles ($<20°$), the assumption of a plane wave incidence is no longer valid, but nevertheless azimuthal angles can be also determined with an accuracy of 10° in the range of incident angles greater than 30° when the wave signal arrives at the station as a spherical wave (NISHINO *et al.*, 1980).

Taking account of the relation of the data-processing time with spatial and temporal variations in the arrival direction of auroral hiss, it is required to improve the accuracy and reliability of the present DF system. Another important practical problem is how to operate the observing system more stably at an unmanned station in Antarctica.

Acknowledgments

This research was sponsored by the National Institute of Polar Research, Japan. Thanks are due to Professor T. NAGATA, Director of the Institute, for his incessant encouragement and strong support to this research. The authors also acknowledge Professor J. OHTSU and Dr. M. HAYAKAWA of the Research Institute of Atmospherics, Nagoya University for their valuable discussion. Two of the authors (M. N. and T. H.) wish to express their gratitude to the kind cooperation given by the wintering members of the nineteenth Japanese Antarctic Research Expedition for the construction and maintenance of the DF system in Antarctica.

References

DELLOUE, J., GARNIER, M., GLANGEAUD, F. and BILDSTEIN, P. (1963): La polarisation des sifflements radioelectriques en relation avec leur direction d'arrivée. C. R. Acad. Sci., **257**, 1131–1133.

ELLIS, G. R. A. and CARTWRIGHT, C. A. (1959): Directional observations of noise from the outer atmosphere. Nature, **184**, 1307–1308.

MAKITA, K. (1979): VLF-LF hiss emissions with aurora. Mem. Natl Inst. Polar Res., Ser. A (Aeronomy), **16**, 126 p.

NISHINO, M., IWAI, A., TANAKA, Y. and YAMAGUCHI, T. (1980): Santen zikansa keisoku ni yoru ôrora-hisu no tôrai hôkô sokutei (Direction finding for auroral VLF hiss based on the measurement of time difference among three spaced points). Denshi Tsûshin Gakkaishi (Trans. IECE), J-64B, **4**, 333–340.

OGUTI, T. (1975): Hiss emitting auroral activity. J. Atmos. Terr. Phys., **37**, 761–768.

TANAKA, Y. (1972): VLF hiss observed at Syowa Station, Antarctica. Proc. Res. Inst. Atmos., Nagoya Univ., **19**, 33–61.

TSURUDA, K. and HAYASHI, K. (1975): Direction finding technique for elliptically polarized VLF electromagnetic waves and its application to the low-latitude whistlers. J. Atmos. Terr. Phys., **37**, 1193–1202.

(*Received July 2, 1980*)